Bearing Capacity for Spatially Random Soil Considering Cone Penetration Test Locations

Marcin Chwała[1]

[1] Wroclaw University of Science and Technology, Department of Geotechnics and Hydrotechnics, Faculty of Civil Engineering, Wybrzeże Wyspiańskiego 27, 50-370 Wrocław, Poland,
E-mail: marcin.chwala@pwr.edu.pl

Abstract: A new approach for 3-D random bearing capacity evaluation for rectangular footings is described. A crucial factor, the soil strength properties spatial variability, was considered in the analyses. The proposed method introduces the locations of CPT tests and considers their impact on foundation reliability. The undrained shear strength of the soil was modelled using a random field, which was discretized via Vanmarcke's spatial averaging approach to single random variables. Those random variables correspond to particular slip surfaces or volumes in the failure mechanism. The Shield-Drucker 3-D failure mechanism was selected as a deterministic background; it was adapted to the probabilistic analyses. Simulated annealing was used to optimize the failure geometry. Numerical analyses were performed for a variety CPT locations and isotropic and anisotropic correlation structures for undrained shear strength. Soil strength properties spatial variability was considered in three directions. However, the same values for the horizontal fluctuation scales were assumed for both horizontal directions. The importance of proper evaluation of vertical and horizontal fluctuation scales and their impact on foundation reliability assessment are shown and discussed.

Keywords: Reliability; spatial variability; horizontal fluctuation scale; kinematical approach; bearing capacity.

1 Introduction

Probabilistic approaches are currently used extensively in a wide range of geotechnical applications. Random bearing capacity evaluations of shallow foundations have been important in recent studies pertaining to the influence of soil strength properites spatial variability (Fenton and Griffiths 2008; Huang et al. 2013; Simoes et al. 2014; Puła and Zaskórski 2015). However, most existing methods have been applied to two-dimensional issues (plane strain conditions), which are simplifications of three-dimensional problems. Those simplifications can significantly affect the results when the soil spatial variability is not considered in the third direction. The lack of three-dimensional probabilistic analyses of shallow foundation bearing capacity can be caused by insufficient computational efficiency. As a result, more efficient methods are necessary to estimate the foundation random bearing capacity for three-dimensional issues. One possibility is to utilize a kinematical approach in accordance with Vanmarcke spatial averaging, an algorithm dedicated to two-dimensional problems was proposed by Puła and Chwała (2018). The corresponding algorithm for three-dimensional issues was presented by Chwała (2019). It is widely accepted that one can obtain the characteristics of a random field that describe soil spatial variability from CPT soundings. Recent applications of conditional random fields in geotechnics are also based on Kriging (Lloret-Cabot et al. 2012; Li et al. 2015).
The approach given by Chwała (2019) is extended in this study to allow the consideration of CPT locations. The presented approach is a new method for conditioning the random field by locations of CPT. As an numerical example, the rectangular footing for variety of CPT locations and variety of correlation structures in random fields (which describe soil strength spatial variability) were analyzed. The proposed method is found to be appropriate for efficient estimations of random bearing capacity characteristics for three-dimensional shallow foundation problems for the undrained conditions.

2 Numerical algorithm

2.1 Probabilistic three-dimensional failure mechanism

The Shield-Drucker type of failure mechanism for rough footing was used as a deterministic background. The deterministic version of the failure mechanism was described by Gourvenec et al. (2006). In this study, its probabilistic equivalent described in Chwała (2019), was used. The geometry of the considered failure mechanism was modified to enable the bearing capacity calculation; different undrained shear strengths were applied for slip surfaces. According to the optimization procedure based on the simulated annealing method (Kirkpatrick et al. 1984), the optimal geometry of failure was determined (i.e., the geometry for which the lowest bearing capacity is obtained). These procedures are the starting point for this study, and they are described in detail in Chwała (2019). The geometry of the probabilistic version of the failure mechanism is shown in Fig. 1.

Proceedings of the 7th International Symposium on Geotechnical Safety and Risk (ISGSR)
Editors: Jianye Ching, Dian-Qing Li and Jie Zhang

Published by Research Publishing, Singapore.
ISBN: 978-981-11-2725-0; doi:10.3850/978-981-11-2725-0_IS10-7-cd

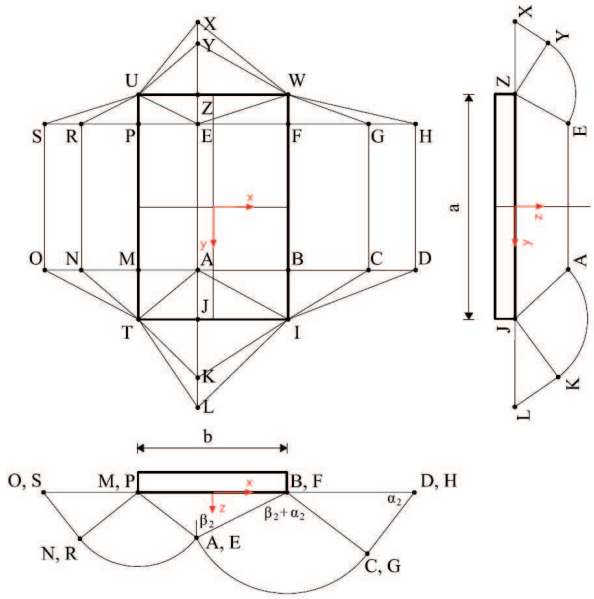

Figure 1. Probabilistic version of the three-dimensional failure mechanism for rectangular footing (more details appear in Chwała (2019)).

2.2 Extended covariance matrix

The method developed by Puła and Chwała (2018) depends on discretization of a random field to single random variables according to the Vanmarcke (1977, 1983) approach. The resulting single random variables describe averaged soil strength parameters on specific slip surfaces. The correlation structure in the initial random field was replaced by a covariance matrix for those single random variables. Due to the assumption of a stationary random field, the mean values of the random variables are equal to the mean value of the initial random field; however, their variance is reduced. For the known covariance matrix, the algorithm based on Cholesky decomposition is used to generate correlated soil strength parameters on each slip surface (see Puła and Chwała (2018) or Chwała (2019)). For the three-dimensional failure mechanism, described in Section 2.1, the initial random field is discretized to surfaces and volumes. In such a case, the covariance matrix is 30×30 in size. However, in this study the author proposes an extension of the framework noted above to consider the CPT location in the bearing capacity evaluation. To make it possible within the framework of the developed approach, the following assumptions have to be made. The first is related to the characteristics of the random field that describe the undrained shear strength; namely, that the mean value, variance and fluctuation scales are known. The proposed method is not based on determining the fluctuation scales from the CPT soundings. The second assumption (which is not mandatory but is used in the numerical example in this study) is that the mean value of the undrained shear strength on the CPT profile is equal to the mean value of the initial random field. Therefore, the average undrained shear strength is known for the CPT profile direction and the formulas given in Eq. (1) and Eq. (3) for the covariance matrix components can be derived. Here, as an example, only derivation of two formulas and its graphical illustration are given. However, all of the necessary formulas were derived by the author for the purpose of the numerical algorithm. This study focuses on general situation shown in Fig. 2a; the location of one CPT can be selected to be arbitrary. However, in the numerical example only locations with $y_0 = 0$ are considered. The cross-section in the x-z plane is shown in Fig. 2b. According to the parameterization shown in Fig. 3a, the following formula for the covariance between the averaged undrained shear strength on the slip surface ABFG and the line of CPT can be derived by assuming a Gaussian covariance function and using the Vanmarcke averaging approach (Eq. 1).

$$\mathrm{Cov}(X_{\mathrm{ABFG}}, X_{\mathrm{CPT}}) = \frac{\sigma_X^2}{P_{\mathrm{ABFG}}} \int_0^{|AB|} \int_{y_F}^{y_A} \exp\left[-\left(\frac{y-y_0}{\omega_y}\right)^2\right] \exp\left[-\left(\frac{x_B - t\cos\left(\frac{\pi}{2}-\beta_2\right)-x_0}{\omega_x}\right)^2\right] \mathrm{d}t\mathrm{d}y \quad , \tag{1}$$

where P_{ABFG} is the area of the rectangular surface ABFG, x_B is the x-coordinate of point B and ω_y and ω_x are equal to $\theta_x/\sqrt{\pi}$ and $\theta_y/\sqrt{\pi}$, respectively. θ_x and θ_y are the horizontal fluctuation scales in the x and y directions. It is assumed that $\theta_x = \theta_y = \theta_h$. Note that parameter t varies from 0.0 to $|AB|$, and y varies from y_F to y_A. The covariance between the considered CPT location and the volume ABC-EFG is derived. According to Fig. 3b, the following parameterization can be introduced:

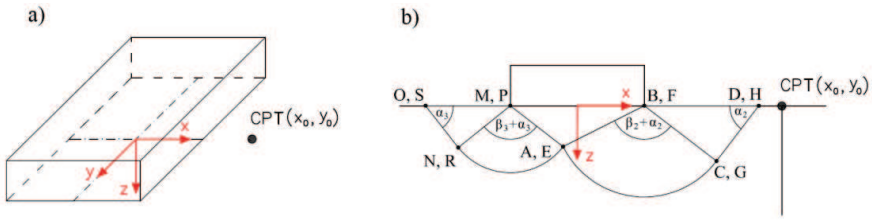

Figure 2. Rectangular footing and exemplary location of CPT (a); cross-section in the x-z plane (b).

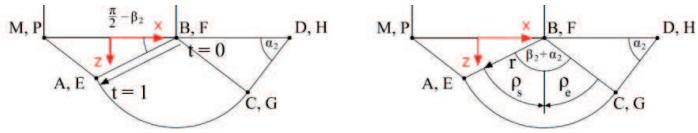

Figure 3. Parameterization of the ABFG slip surface (a); parameterization of the ABC-EFG region (b).

$$\begin{aligned} x &= x_B + r\sin\rho \\ y &= y \\ z &= r\cos\rho \end{aligned} \tag{2}$$

By using Eq. (2), the following formula for the considered covariance can be derived:

$$\mathrm{Cov}(X_{\mathrm{ABC-EFG}}, X_{\mathrm{CPT}}) = \frac{\sigma_X^2}{V_{\mathrm{ABC-EFG}}} \int_0^{|AB|} \int_{y_E}^{y_A} \int_{-\rho_s}^{\rho_e} \exp\left[-\left(\frac{y-y_0}{\omega_y}\right)^2\right] \exp\left[-\left(\frac{x_B + r\sin\rho - x_0}{\omega_x}\right)^2\right] r\,dr\,dy\,d\rho \quad , \tag{3}$$

where $V_{\mathrm{ABC-EFG}}$ is the volume of the region ABC-EFG; ρ_s and ρ_e are defined in Fig. 3b. The considered three-dimensional failure mechanism consists of 30 dissipation regions. Therefore, the addition of the one CPT to the covariance matrix boosts its dimension by one; therefore, after considering an additional CPT, the final size of the covariance matrix will be 31×31. The covariance matrix is symmetrical. Therefore, 30 new covariances between CPT and all dissipation regions have to be derived. Two examples of new covariances are given above. As a result, the covariance matrix can be represented as in Eq. (4).

$$[C_X] = \begin{bmatrix} 1.0 & C(r_1,\mathrm{CPT}) & C(r_2,\mathrm{CPT}) & C(r_3,\mathrm{CPT}) & C(r_4,\mathrm{CPT}) & & C(o_8,\mathrm{CPT}) & C(o_9,\mathrm{CPT}) & C(o_{10},\mathrm{CPT}) \\ C(r_1,\mathrm{CPT}) & V(r_1) & C(r_1,r_2) & C(r_1,r_3) & C(r_1,r_4) & & C(r_1,o_8) & C(r_1,o_9) & C(r_1,o_{10}) \\ C(r_2,\mathrm{CPT}) & C(r_1,r_2) & V(r_2) & C(r_2,r_3) & C(r_3,r_4) & \cdots & C(r_2,o_8) & C(r_2,o_9) & C(r_2,o_{10}) \\ C(r_3,\mathrm{CPT}) & C(r_1,r_3) & C(r_2,r_3) & V(r_3) & C(r_3,r_4) & & C(r_3,o_8) & C(r_3,o_9) & C(r_3,o_{10}) \\ C(r_4,\mathrm{CPT}) & C(r_1,r_4) & C(r_3,r_4) & C(r_3,r_4) & V(r_4) & & C(r_4,o_8) & C(r_4,o_9) & C(r_4,o_{10}) \\ & & \vdots & & & \ddots & & \vdots & \\ C(o_8,\mathrm{CPT}) & C(r_1,o_8) & C(r_2,o_8) & C(r_3,o_8) & C(r_4,o_8) & & V(o_8) & C(o_8,o_9) & C(o_8,o_{10}) \\ C(o_9,\mathrm{CPT}) & C(r_1,o_9) & C(r_2,o_9) & C(r_3,o_9) & C(r_4,o_9) & \cdots & C(o_8,o_9) & V(o_9) & C(o_9,o_{10}) \\ C(o_{10},\mathrm{CPT}) & C(r_1,o_{10}) & C(r_2,o_{10}) & C(r_3,o_{10}) & C(r_4,o_{10}) & & C(o_8,o_{10}) & C(o_9,o_{10}) & V(o_{10}) \end{bmatrix} \tag{4}$$

In Eq. (4), a shortened denoting convention was used. The covariance and variance were denoted by $C(\,)$ and $V(\,)$, respectively. All of the dissipation regions were denoted as given in Table 1.

2.3 Numerical algorithm

The algorithm proposed in this study is consistent with those proposed earlier (Puła & Chwała 2018; Chwała 2019); however, it encompasses several important differences. The algorithm makes it possible to assume the variance of the mean value of the undrained shear strength resulting from the CPT sounding. In general, this variance is significantly lower than the variance of the initial random field. Basing on the information given in Section 2.2 and the method described in Puła and Chwała (2018) and Chwała (2019), the following five primary steps can be defined:

Step 1. Generate, from a lognormal distribution, a mean value of the undrained shear strength on the considered CPT line based on μ and σ_{CPT}.
Step 2. Generate independent values of the undrained shear strength ($c_1, \ldots, c_{30}$) from a lognormal distribution for each dissipation region based on μ and σ.
Step 3. Determine an optimal failure geometry for undrained shear strengths from Step 2 (a detailed algorithm is provided in Chwała (2019).
Step 4. Determine the extended covariance matrix (Eq. (4)). Calculate the new undrained shear strengths (averaged and conditioned by the location of CPT) according to the extended covariance matrix and values from Steps 1 and 2.
Step 5. Determine the optimal failure geometry for the averaged undrained shear strengths from Step 4. The corresponding bearing capacity is the result of one realization.
Step 6. Repeat steps 1–5 *N* times in a framework of the Monte Carlo method.

μ and σ refer to the mean value and variance for a lognormal distribution, respectively; σ_{CPT} is the variance of CPT mean value (related to CPT accuracy).

Table 1. Conventions for naming the dissipation regions used in Eq. (4).

Dissipation region	Denoting convention	Dissipation region	Denoting convention	Dissipation region	Denoting convention
ABFE	r_1	UEP	t_7	ABC-EFG	o_1
DCHG	r_2	USR	t_8	AMN-EPR	o_2
AMEP	r_3	IAJ	t_9	EFG-W	o_3
NORS	r_4	TAJ	t_{10}	ABC-I	o_4
ABI	t_1	IKL	t_{11}	EPR-U	o_5
ICD	t_2	TKL	t_{12}	AMN-T	o_6
EFW	t_3	WEZ	t_{13}	AKJ-I	o_7
GWH	t_4	WXY	t_{14}	AKJ-T	o_8
TAM	t_5	UEZ	t_{15}	EYZ-W	o_9
TON	t_6	UXY	t_{16}	EYZ-U	o_{10}

3 Numerical example

A rectangular footing with $a = 2.0$ m and $b = 1.0$ m (Fig. 4) was examined. Six CPT locations were considered. For each one, $y_0 = 0.0$ m, and x_0 varies from 0.0 m to 10.0 m. The view from the top of the described locations is shown in Fig. 4. The vertical fluctuation scale is assumed to be equal $\theta_z = 1.0$ m; for each point P_i, numerical analysis was performed for the following horizontal fluctuation scales: $\theta_h = 1.00$ m, 1.50 m, 2.00 m, 3.75 m, 5.00 m, 7.50 m, 10.00 m, 15.00 m, 20.00 m and 30.00 m. Due to the preliminary nature of the presented analysis, the same number of Monte Carlo realizations were assumed for each considered issue (i.e., $N = 500$).

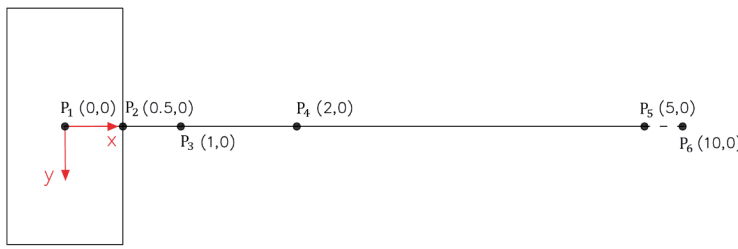

Figure 4. CPT location considered in the numerical example. Note that point P_6 is not drawn to scale.

4 Results

As noted in Section 3, six series of analysis were performed involving 60 tasks. The results are shown in Fig. 5; panels a and b show the standard deviations and mean values of bearing capacity, respectively. Both the standard deviations and mean values are plotted versus a horizontal fluctuation scale. In Fig. 5a, a strong dependence of the bearing capacity standard deviation on horizontal fluctuation scale and CPT location can be seen. In most cases, for a constant horizontal fluctuation scale, the bearing capacity standard deviation decreases as the CPT location approaches the center of the footing. However, for the specified CPT location the bearing capacity standard deviation attains a maximum value. The location of the maximum depends on the distance of the CPT from the footing center and increases with increasing distance. Namely, for point P_1 the maximum standard deviation is observed for $\theta_h = 1.5$ m; however, for point P_6 the maximum is observed for $\theta_h = 10$ m. This behaviour of the bearing capacity standard deviations is the result of two primary factors: the first one is related to the fact that for an unconditioned random field a larger horizontal fluctuation scale results in a larger bearing capacity standard deviation. However, for issues conditioned by the CPT location, a larger horizontal fluctuation scale yields a stronger correlation; therefore, the observed standard deviation of the bearing capacity is reduced. The variability of the bearing capacity mean values is much smaller; the mean values increase slowly with an increase in the horizontal fluctuation scale. However, the worst-case correlation length (Fenton and Griffiths 2008) is observed for $\theta_h \approx 1.5$ m (Fig. 5b). Slightly larger (by 1–3%) mean bearing capacity values are observed for points located closer to the center of the footing.

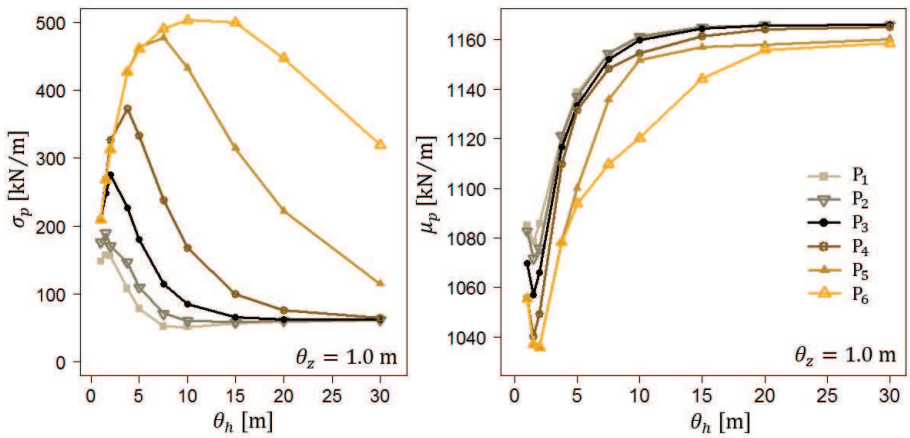

Figure 5. Bearing capacity standard deviations (a); bearing capacity mean values (b). The results are for a rectangular footing measuring 2×1 m.

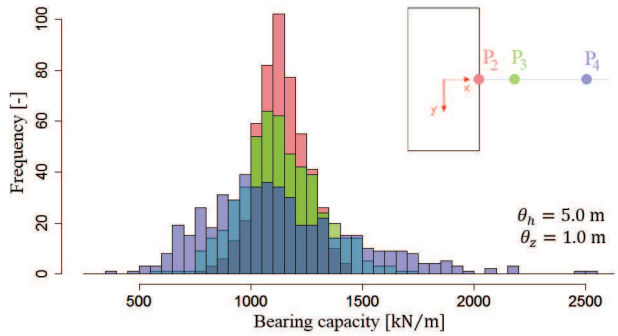

Figure 6. Bearing capacity histograms obtained for $\theta_v = 1.0\ m$, $\theta_h = 5.0\ m$ and CPT locations determined by points: P_2, P_3 and P_4.

A comparison of the three selected bearing capacity histograms is shown in Fig. 6. A decreasing trend in bearing capacity standard deviation is clearly observed for CPT locations closer to the footing center.

5 Conclusions

The author has proposed an efficient new algorithm to estimate the bearing capacity for rectangular footings that takes into account CPT location. The method presented in this study is an extension of the algorithm proposed for rectangular footings (Chwała 2019). The preliminary numerical analyses presented in this study indicate a strong dependence of CPT location on bearing capacity standard deviation. The proposed approach simplifies the problem because only the average value of the CPT profile line (or another testing method) is introduced. It is important to note that the approach is not dedicated to determining fluctuation scales from CPT tests (Lloret-Cabot et al. 2014; Ching et al. 2018). However, the method is promising because it results in high efficiency and the ability to include a larger number of soil soundings; both aspects are crucial for practical applications. The presented approach can be inverted in a way that a CPT location can be determined to minimize the bearing capacity standard deviation. Thanks to the high efficiency of this method, which still can be improved, problems with complex foundation systems can be solved. Such work should be an objective for future studies.

Acknowledgements

The author is grateful for the support by National Science Centre (grant: Miniatura 2; Project No. 2018/02/X/ST8/02939)

References

Ching J., Wu T. J., Stuedlein A. W., Bong T. (2017). *Estimating horizontal scale of fluctuation with limited CPT soundings*. Geoscience Frontiers, Vol. 9, 6, 1597-1608.

Chwała M. (2019). *Undrained bearing capacity of spatially random soil for rectangular footings*. Submitted to Soils and Foundations.

Fenton GA, Griffiths DV. *Risk assessment in geotechnical engineering*. Wiley; 2008.

Gourvenec S., Randolph M., Kingsnorth O. (2006). *Undrained Bearing Capacity of Square and Rectangular Footings*. International Journal of Geomechanics, Vol. 6, 3, 147-157.

Huang J., Lyamin A. V., Griffiths D. V., Sloan S. W., Krabbenhoft K., Fenton G.A. (2013). *Undrained bearing capacity of spatially random clays by finite elements and limit analysis*. Proceedings of the 18th ICSMGE, Paris, 731-734.

Kirkpatrick S., Gelatt C. D., Vecchi M. P. (1983). *Optimization by Simulated Annealing*. Science, 220, 671-680.

Li X. Y., Zhang L. M., Li J. H. (2015). *Using conditioned random field to characterize the variability of geologic profiles*. Journal of Geotechnical and Geoenvironmental Engineering, 142(4).

Lloret-Cabot M., Hicks M. A., Van Den Eijnden A. P. (2012). *Investigation of the reduction in uncertainty due to soil variability when conditioning a random field using Kriging*. Geotechnique Letters 2, 123-127.

Lloret-Cabot M., Fenton G. A., Hicks M. A. (2014). *On the estimation of scale of fluctuation in geostatistics*. Georisk: Assessment and Management of Risk for Engineered Systems and Geohazards, 8:2, 129-140.

Puła W., Zaskórski Ł. (2015). *On some methods in safety evaluation in geotechnics*. Studia Geotechnica et Mechanica, 37(2), 17-32.

Puła W., Chwała M. (2018). *Random bearing capacity evaluation of shallow foundations for asymmetrical failure mechanisms with spatial averaging and inclusion of soil self-weight*. Computers and Geotechnics, 101, 176-195.

Shield R. T., Drucker D.C. (1953). *The application of limit analysis to punch-indentation problems*. Journal of Applied Mechanics, 20, 453-460.

Simoes J. T., Neves L. C., Antao A. N., Guerra N. M. C. (2014). *Probabilistic analysis of bearing capacity of shallow foundations using three-dimensional limit analyses*. International Journal of Computational Methods, Vol. 11, No. 02, 1342008-1-20.

Vanmarcke E. H. (1977). *Probabilistic modelling of soil profiles*. Journal of the Geotechnical Engineering Division. Vol. 103, 11, 1227–46.

Vanmarcke E. H. (1983). *Random fields – analysis and synthesis*. Cambridge: MIT Press.